Published in final edited form as:
Cancer Res. 2011 August 15; 71(16): 5522–5534. doi:10.1158/0008-5472.CAN-10-3143.

CXCL12/CXCR4 blockade induces multimodal anti-tumor effects that prolong survival in an immunocompetent mouse model of ovarian cancer

Elda Righi[#1,2], **Satoshi Kashiwagi**[#1], **Jianping Yuan**[1], **Michael Santosuosso**[1], **Pierre Leblanc**[1], **Rachel Ingraham**[1], **Benjamin Forbes**[1], **Beth Edelblute**[1], **Brian Collette**[1], **Deyin Xing**[3], **Magdalena Kowalski**[1,4], **Maria Cristina Mingari**[2], **Fabrizio Vianello**[5], **Michael Birrer**[6], **Sandra Orsulic**[3,8], **Glenn Dranoff**[7], and **Mark C. Poznansky**[1]

[1]Vaccine and Immunotherapy Center, Infectious Diseases Medicine, Massachusetts General Hospital, Charlestown, MA

[2]Department of Experimental Medicine and IST Cancer Research, Genoa University, Italy

[3]Molecular Pathology, Massachusetts General Hospital, Boston, MA

[4]Department of Zoology, Clare College, Cambridge, UK

[5]Dept of Haematology, Padua University Hospital, Italy

[6]Gynecological Oncology Cancer Center, Massachusetts General Hospital, Boston, MA

[7]Department of Medical Oncology and Cancer Vaccine Center, Dana-Farber Cancer Institute, Boston, MA

[8]Women's Cancer Research Institute, Cedars-Sinai Medical Center, Los Angeles, CA

[#] These authors contributed equally to this work.

Abstract

The chemokine CXCL12 and its receptor CXCR4 are expressed widely in human cancers including ovarian cancer, where they are associated with disease progression at the levels of tumor cell proliferation, invasion, and angiogenesis. Here we used an immunocompetent mouse model of intraperitoneal papillary epithelial ovarian cancer to demonstrate that modulation of the CXCL12/CXCR4 axis in ovarian cancer has multimodal effects on tumor pathogenesis associated with induction of antitumor immunity. siRNA-mediated knockdown of CXCL12 in BR5-1 cells that constitutively express CXCL12 and CXCR4 reduced cell proliferation in vitro and tumor growth in vivo. Similarly, treatment of BR5-1-derived tumors with AMD3100, a selective CXCR4 antagonist, resulted in increased tumor apoptosis and necrosis, reduction in intraperitoneal dissemination, and selective reduction of intratumoral FoxP3+ regulatory T-cells (T-regs). Compared to controls, CXCR4 blockade greatly increased T cell-mediated antitumor immune responses, conferring a significant survival advantage to AMD3100-treated mice. In addition, the selective effect of CXCR4 antagonism on intratumoral T regulatory cells was associated with both higher CXCR4 expression and increased chemotactic responses to CXCL12, a finding that was also confirmed in a melanoma model. Together, our findings reinforce the concept of a critical role for the CXCL12/CXCR4 axis in ovarian cancer pathogenesis, and they offer a definitive preclinical validation of CXCR4 as a therapeutic target in this disease.

Corresponding authors: Elda Righi and Mark C. Poznansky, Vaccine and Immunotherapy Center, Infectious Diseases Medicine, Massachusetts General Hospital (East), Charlestown, MA 02129, Phone: 617-724-6375, erighi@partners.org, mpoznansky@partners.org.

Keywords

CXCL12/CXCR4 axis; AMD3100; tumor progression

Introduction

Chemokines and their cognate receptors have been shown to play a role in favoring tumor growth, progression and immune escape through multiple mechanisms(1-6). CXCL12 and its receptor, CXCR4, constitute a chemokine-receptor axis that is known to be expressed in various tumors and to correlate with poor clinical outcome(7-14). CXCL12 is expressed by primary human ovarian cancer and has been detected in tumor tissue and ascitic flui (2,15,16), while CXCR4 is the only chemokine receptor shown to be constitutively expressed in epithelial ovarian cancer(15,16). CXCL12 can stimulate ovarian cancer cell proliferation by direct activation of protein kinases PKB and MAPK, and by indirect protection of cancer cells from apoptosis (16-18).

CXCL12 produced by tumor tissue and surrounding stroma stimulates VEGF-mediated angiogenesis(5, 19) and the recruitment of endothelial progenitor cells from the bone marrow(20). CXCL12 can also mediate tumor invasion and metastasis by impairing cell adhesion to integrins, attracting CXCR4+ cancer cells and increasing matrix metalloproteinase expression(8, 15,16,21). CXCL12 has also been demonstrated to repel tumor-specific effector T-cells and to recruit suppressive cell populations at tumor sites, including IL-10-producing plasmacytoid dendritic cells, T-regs, and myeloid-derived suppressor cells (MDSCs)(22-25).

We proposed that modulation of the CXCL12/CXCR4 axis in ovarian cancer would impact multiple aspects of tumor pathogenesis including immune dysregulation. Therefore this ligand/receptor axis would provide an attractive therapeutic target. The availability of an immune competent murine model of intraperitoneal papillary epithelial ovarian cancer derived from a syngeneic cell line that constitutively expresses CXCL12 and CXCR4 and the existence of a clinically validated, highly specific CXCR4 antagonist, AMD3100, facilitated this approach(26, 27). To date, AMD3100 has been tested in vivo in ovarian cancer in the context of its impact on tumor growth and dissemination in immune deficient mice(21). Knocking down CXCL12 expression or CXCR4 blockade with AMD3100 led to increased tumor cell apoptosis and reduction in tumor growth, peritoneal dissemination and angiogenesis. CXCR4/CXCL12 blockade also lead to a selective reduction in intratumoral T-regs as compared to CD8+ T-cells and increased anti-tumor immunity. These anti-tumor effects were associated with significantly prolonged survival. The selective effect of CXCR4/CXCL12 blockade on intratumoral T-regs was associated with significantly greater expression of CXCR4 and chemotactic responses to CXCL12 of this T-cell subpopulation compared to CD8+ T-cells. These findings support the critical role of the CXCL12/CXCR4 axis in ovarian cancer pathogenesis and immune evasion and provide validation for a new therapeutic target in this disease.

Methods

Animal models and cell lines

Tumor generation involved a single intraperitoneal injection of the syngeneic cancer cell line, BR5-1(1×10^7 cells per mouse), into five-week-old FVB/NJ mice(Bar Harbor, ME)(28), and was consistently first evident after three to five weeks via abdominal distension secondary to malignant ascites. Tumor-bearing mice were euthanized at the endpoint when there were signs of distress, including fur ruffling, rapid respiratory rate, hunched posture,

reduced activity, and progressive ascites formation. At necropsy, tumor weight, volume of ascites, and peritoneal dissemination were measured and lungs, brain, and liver were examined for metastasis by visual inspection. A second tumor model, B16F10 murine melanoma, was used as described previously re described (see Supplemental Methods)(29). All measurements were performed in a blinded manner, (to control or experimental group), and all animal experiments were executed according to Public Health Service Policy on Humane Care of Laboratory Animals and were approved by the Institutional Animal Care and Use Committee of Massachusetts General Hospital.

CXCL12 knockdown using RNAi vector

CXCL12 expression knockdown in BR5-1 cells was achieved by transducing the cells with MISSION lentiviral transduction particles (Sigma-Aldrich) through the use of five different shRNA sequences targeting CXCL12 (see Supplemental Methods).

Cell proliferation and CXCL12 quantitation

Cell proliferation was measured by mannual counting and by using the Premix WST-1 Cell Proliferation Assay System(Clontech Laboratories, Mountain View, CA). In certain experiments, 100 ng/ml of exogenous recombinant murine CXCL12(Peprotech, Rocky Hill, NJ) was added to the culture of CXCL12 knocked-down BR5-1 cells(kdBR5-1) in fresh media at 0, 24, 48, and 72 hr. CXCL12 was measured in cancer cell culture supernatants using a CXCL12-ELISA kit(R&D).

AMD3100 treatment in vivo

Administration of AMD3100 into mice was achieved using osmotic minipumps(Alza, Palo Alto, CA) implanted dorsolaterally under the skin. For the murine ovarian cancer model, animals were treated with AMD3100 or vehicle (PBS) using two different schedules; schedule A - treatment began upon the development of ascites either for 3 days (for time-matched study) or until evident signs of distress as described above (for survival study), schedule B - treatment began two weeks after intraperitoneal injection of tumor cells either for 14 days (for time-matched study) or until evident signs of distress as described above (for survival study). For the murine B16F10 melanoma model, AMD3100 treatment was initiated when tumors reached 4 mm in mean diameter either for 4 days (for time-matched study) or until tumors reached a size >12mm in diameter or the mice showed signs of distress (for survival study). The details of the treatment are described in the Supplemental Methods. All monitoring of animal survival and tumor progression was performed in a manner that was blinded to the observer.

Quantitation of tumor vessel density by immunofluorescence

Mice were euthanized at day 3 after tumor development, at which point the sizes of the tumors analyzed were comparable in the treatment group vs. controls. Tumor vessel density was determined and scored in a blinded manner using fluorescein-labeled lectin (Vector lab, Burlington, MA) and image analysis(Carl Zeiss LSM5 Pascal, Carl Zeiss North America, MO Zeiss) and Image J 1.43 freeware(NIH, MD) as previously described(30).

Quantitation of tumor infiltrating lymphocytes (TILs) by immunofluorescence

Immunofluorescence analysis of tumor infiltrating CD8(CTLs) and FoxP3(T-regs) positive cells was performed. T-cells were visualized using confocal microscopy and scored in a blinded manner using Image J 1.43 freeware (see Supplemental Methods).

Quantitation of apoptosis using TUNEL staining

TUNEL taining was performed on 10μm-thick tumor sections prepared as described in the previous section using the In situ Cell Death Detection Kit TMR Red(Roche). Slides were imaged and analyzed using Image J and were blinded to the analyzer.

Flow cytometry

For TIL subpopulation analysis, mononuclear cells including tumor cells, stromal cells and immune cells derived from disaggregated tumor tissue were separated by centrifugation on Ficoll Hypaque, and directly stained with fluorophore-conjugated anti-CD3, anti-CD8, anti-CD4, anti-CD25, anti-FoxP3, and anti-CXCR4 antibodies(BD Bioscience). Cell subpopulations, including CD3+CD4+ T helper cells, CD3+CD8+ cytotoxic T-cells(CTL) and CD4+CD25+FoxP3+(T-regs) were quantified as a percentage of cell per gram of tumor tissue through examination of both positive control and fluorescence-minus-one gating strategy (FMO)(31). For in vitro assessment of tumor-specific T-cell function, splenocytes and TILs isolated and prepared as single-cell suspensions were plated and pulsed with tumor lysates, Her2/neu peptide(0.1 μg/ml, PDSLRDLSVF, EZBiolab, Westfield, IN)(32), or medium alone for 18 hr when Golgi Plug(BD Bioscience) was added (0.75 μl/well) for 6 hr, stained with anti-Granzyme B(R&D Systems) , and analyzed on a 3 laser LSRII BD Biosciences)(see Supplemental Methods).

T regulatory cell depletion and CD8+ cell isolation

Magnetic beads were used to separate T-regs and CD8+ cells (MACS, Milteny Biotech, Auburn, CA) yielding a population with >95% purity. T-reg depleted cells(CD4+CD25-) were plated, stimulated and stained as described above.

Transmigration assay

T-regs and CD8+ cell migration was measured using Transwells (96-well format, 3-micron pore size; ChemoTx System, Neuro Probe Inch, Gaithersburg, MA) as previously described(33) in CXCL12 concentrations(5ng/ml, 50ng/ml, 500ng/ml, and 5μg/ml), and in the presence or absence of AMD3100(1μg/ml) or pre-incubation with 100 ng/ml pertussis toxin(PTX; Sigma) for 1hr at 37°C.

Statistical analysis

All of the results are expressed as mean ± SEM. Differences between treatment groups were determined by the Mann Whitney test and in other numerical variables by unpaired *t* test with a *P* value of <0.05 considered significant. All statistical analyses were independently performed on datasets by Dr. Gebremichael at the Harvard School of Public Health.

Results

CXCL12 knockdown impacts BR5-1 proliferation in vitro and tumor growth in vivo

CXCL12 has been shown to stimulate ovarian cancer cell proliferation in vitro(16). We used the murine ovarian cancer cell line BR5-1, which constitutively expresses CXCL12 and CXCR4, to observe the effect of RNAi-mediated CXCL12 silencing on tumor growth. CXCL12 levels from wild-type BR5-1 cells(wtBR5-1), RNAi-transfected, CXCL12 knocked-down BR5-1 cells(kdBR5-1), and scrambled-RNAi transfected BR5-1 cells(scrBR5-1) were quantitated using an ELISA immunoassay(Figure 1A). Similar levels of CXCL12 were released by wtBR5-1 and scrBR5-1 (1.05 ± 0.19 ng/ml and 0.85 ± 0.09 ng/ml) while CXCL12 from kdBR5-1 was negligible (<0.02 ng/ml, $P < 0.0001$). CXCR4 expression was not significantly different among wtBR5-1, kdBR5-1, and scrBR5-1 (Figure 1B). KdBR5-1 proliferated at a significantly slower rate compared to wtBR5-1 and

scrBR5-1 ($P < 0.0001$, Figure 1C). The results were confirmed using a WST-1 proliferation assay, showing a significantly higher absorbance in wtBR5-1 compared to kdBR5-1 at 48 hr (absorbance ratio 12.5 ± 0.23 vs. 3.37 ± 0.30 respectively, $P < 0.001$, not shown). Addition of exogenous CXCL12 significantly increased kdBR5-1 proliferation to a level comparable to wild type (Figure 1D). Apoptosis was excluded as a mechanism responsible for the reduced kdBR5-1 cell proliferation (Figure 1E), thus confirming direct effect of CXCL12 on ovarian cancer cell proliferation(16).

To test if defective CXCL12 production was maintained in vivo, cancer cells derived from wtBR5-1(WT) and kdBR5-1 tumors(RNAi) were grown for 48 hr in media. Quantitation of CXCL12 in supernatants showed results comparable to in vitro data, with CXCL12 < 0.02 ng/ml in tumor cells extracted from kdBR5-1 injected mice and CXCL12 levels of 1.2 ± 0.10 ng/ml in tumor cells extracted from wtBR5-1 tumors. Furthermore, RNAi tumors displayed a marked reduction of CXCL12 (stained red in Figure 1F) compared to WT tumors via immunofluorescence. Small numbers of cells expressing CXCL12 were detected and thought to be due to the infiltration of CXCL12-expressing stromal and endothelial cells (white arrows, Figure 1F) in the tumor microenvironment.

FVB/NJ mice injected with wtBR5-1 normally generate intraperitoneal tumors in three to five weeks. The time interval between tumor implantation and appearance of ascites was found to be significantly higher in kdBR5-1 injected mice compared to wtBR5-1 and scr-BR5-1 injected mice (53 ± 5.5 days vs. 33 ± 2.1 and 32 ± 3.3 days respectively, $P < 0.05$, Supplementary Figure 1A). A reproducible '*survival window*' was defined between the first clinical sign of disease (abdominal swelling secondary to ascites formation) and euthanasia required by advanced clinical condition. The overall survival was significantly longer in kdBR5-1-injected mice compared to wtBR5-1-injected mice (8.7 ± 1.8 days vs. 3.4 ± 0.4 days respectively, $P < 0.005$, Figure 1G). Mice injected with scrBR5-1 had similar survival windows (3.3 ± 0.5 days) compared to wtBR5-1-injected mice.

AMD3100 treatment prolongs mouse survival and reduces dissemination of tumors

Mice were treated with AMD3100 either at the onset of ascites until the end-stage time point (schedule A) in order to simulate the treatment in human disease(34), or from day 15 after the implantation of tumor cells (schedule B). AMD3100 treatment schedules were based on previous pharmacokinetic evaluations to maintain steady serum levels (35). AMD3100 treatment on schedule A resulted in a two-fold increase in survival compared to PBS-treated mice (6 days vs. 3 days, $P < 0.05$) (Figure 2A), and higher overall survivals were reported in the AMD3100 treated mice vs. controls, (38 days ± 1.1. vs. 32 days ± 1.5, $P < 0.05$) (Figure 2B). In a separate experiment, AMD3100-treated and PBS-treated mice were euthanized at day three from the onset of clinical signs to compare total tumor mass, volume of ascites, and tumor dissemination (Figure 2 C-E). Mean tumor weight and amount of ascites were lower in AMD-treated compared to PBS–treated mice (1.3 ± 0.23 g and 4.4 ± 0.4 ml vs. 0.8 ± 0.17 g and 3.6 ± 0.4 ml, respectively) (Figure 2 D- E), although these differences were not significant.

BR5-1 injection robustly results in multiple tumor nodules growing on organ surfaces without significant invasion. Sites of tumor spread include the mesothelial lining of the peritoneum, intestines, spleen, and diaphragm, but not the lungs(28). Tumor dissemination was compared between AMD3100-treated vs. PBS-treated mice (Figure 2 F-G) and classified as localized (localizations ≤ 3), limited (6 < localizations > 3, with no visible masses on mesentery and diaphragm), or disseminated (localizations ≥ 6, including mesentery and diaphragm). The percentage of mice with tumor deposits on organ surfaces at necropsy was lower in AMD3100-treated compared to PBS-treated mice. While all

AMD3100-treated mice had localized or limited tumors, 70% of the tumors in PBS-treated mice fell under the disseminated category.

In schedule B, when the treatment was started at day 15 after tumor implantation, a significant delay in the onset of ascites was recorded in the AMD3100 treated mice vs. controls (21 ± 0.5 days vs. 24 ± 1.3 days, $P < 0.05$). An increase in survival in AMD3100 treated versus control treated animals was observed (3.6 days vs. 7 days, Figure 2H) as well as higher overall survival times (41 ± 2.1 days vs. 36 ± 0.5 days, $P < 0.05$) (Supplemental Figure 1B). Tumor dissemination in schedule B examined five weeks after the tumor injection was comparable to those on schecdule A (Figure 2I).

CXCL12/CXCR4 manipulation markedly reduces tumor angiogenesis

CXCL12 is a pro-angiogenic factor in ovarian cancer via upregulation of VEGF, which in turn increases CXCR4 expression by endothelial cells (19, 36). Vessel density was significantly lower in AMD3100 tumors and RNAi tumors compared to PBS-tumors (Figure 3A and B: 91.23 ± 17.57 vessels/mm^2 and 71.11 ± 28.73 vessels/mm^2 vs. 167.84 ± 27.92 vessels/mm^2 respectively, AMD3100 vs. PBS - $P < 0.05$; RNAi vs. PBS - $P < 0.05$). SCR tumors displayed similar vessel density (111.11 ± 11.07 vessels/mm^2) to PBS-tumors.

AMD3100 treatment increases tumor apoptosis and necrosis

It has been previously reported that CXCL12-mediated inhibition of the NF-kB/TNFα apoptotic pathway (17, 18) affords in vivo protection from tumor apoptosis and that this can be impaired via CXCR4 inhibition (37, 38). Here, significantly higher numbers of apoptotic cells were found in AMD3100 tumors compared to PBS-tumors (90.86 ± 17.99 cells/mm^2 vs. 37.18 ± 11.60 cells/mm^2, $P < 0.05$) (Figure 4 A-B). RNAi tumors showed a non significant increase in apoptotic cells compared to controls (97.35 ± 46.5 cells/mm^2), suggesting a compensatory role for stromal-derived CXCL12 in the these tumors. H&E stained selected tumor tissues from AMD3100-treated and PBS-treated mice showed areas of necrosis in 50.0% of the AMD3100 tumor sections, while PBS tumor sections appeared microscopically negative for necrotic tissue (Figure 4C).

CXCR4 antagonism selectively reduces intratumoral FoxP3+ T-cell infiltration in comparison to CD8+ T-cells

CXCL12 can act as both a chemoattractant and a chemorepellent for T-cell subpopulations in a concentration and CXCR4 dependent manner in tumor models(25). Therefore, we examined the effect of the manipulation of the CXC12/CXCR4 axis on intratumoral T-cell trafficking in this model of ovarian cancer. CD8+ T-lymphocyte infiltration was not significantly different in PBS-treated, kdBR5-1-injected, and AMD3100-treated mice via immunofluorescence (Figure 5A, upper panels and 5B) and flow cytometry (CD3+CD8+: 11.09 ± 0.20%, 10.44 ± 1.18 %, 9.54 ± 0.16 % and CD3+CD4+: 42.1 ± 2.39 %, 40.53 ± 0.15 %, 40.33 ± 2.30 %, respectively). In contrast, RNAi tumors and AMD3100 treatment resulted in a significant 4 to 5-fold reduction in FoxP3+ T-cells compared to PBS-tumors as determined by immunohistochemistry (18.77 ± 7.29 cells/mm^2 and 14.46 ± 4.48 cells/mm^2 vs. 76.0 ± 25.02 cells/mm^2, $P < 0.05$, Figure 5A, lower panels and 5C) and flow-cytometry (Figure 5D). No differences were detected in the spleen for CD3+CD8+, CD3+CD4+ and CD4+CD25+FoxP3+ cells among PBS-treated, kdBR5-1-injected, and AMD3100-treated mice (data not shown). In order to determine whether this was the result of selective FoxP3+ T-cell redistribution(39) or an alteration in TIL trafficking(25), thymus and spleens were obtained from tumor-bearing mice and stained for FoxP3 expression. No significant differences were detected in PBS-treated (1008.23 ± 196.15 cells/mm^2 and 69.54 ± 21.77 cells/mm^2) vs. AMD3100-treated mice with regards to the number of FoxP3+ T-cells in these tissues (948.15 ± 156.03 cells/mm^2 and 153.40 ± 86.65 cells/mm^2, Figure 5E).

AMD3100 treatment resulted in a 6-fold increase in the CD8+/FoxP3+ ratio, a parameter correlated with increased survival in ovarian cancer(40), compared to control PBS treated animals (3.12 and 3.50 vs. 0.58 respectively, $P < 0.01$, Figure 5F).

AMD3100 treatment selectively increases tumor-specific T-cell responses and impairs T-reg migration in vitro

To test if the differential distribution of T-regs was associated with impaired tumor-specific T-cell function, we analyzed the in vitro production of Granzyme B in T-lymphocytes extracted from spleen and tumors in AMD3100-treated and PBS-treated mice as described above. Splenocytes and TILs were stimulated with tumor lysates and Her2/neu specific peptide for 24 hr and then analyzed for the intracellular expression of Granzyme B using flow-cytometry. Her2/neu was shown to be expressed by BR5-1 using flow-cytometry (data not shown). Granzyme B production was significantly higher in TILs from AMD3100-treated compared to PBS-treated mice for both tumor lysates and Her2/neu peptide stimulation for CD4+ and CD8+ T-cells (Figure 6 A-B). To assess the impact of T-regs on T-lymphocyte function, splenocytes and TILs were depleted of T-regs using magnetic beads. Depleted CD4+CD25- and non-depleted CD4+CD25+ cells were stimulated as before, and Granzyme B expression was determined using flow cytometry. Non-depleted CD4+ TILs from AMD3100 tumors showed higher Granzyme B production compared to PBS-tumors, whereas T-reg depleted TILs from PBS-tumors demonstrated increased Granzyme B production compared to non-depleted TILs from PBS treated tumors (Figure 6 C-D). No differences in Granzyme B production were observed in the spleen derived T-cell populations for either AMD3100 or PBS-treated tumors (Figure 6D and data not shown).

We observed that intratumoral T-regs consistently express higher CXCR4 levels compared to CD4+CD25− and CD8+ cells (Figure 6E-F). We then examined the migratory responses of T-regs and CD8+ cells to gradients of CXCL12 in vitro. We showed that T-regs from both tumors and spleen underwent chemotaxis in response to chemotactic gradients of the CXCL12 with a classical bell shaped dose-response curve. Addition of AMD3100 or pre-treatment of cells with Pertussis toxin (PTX) significantly impaired G-coupled, CXCR4-mediated T-reg cell chemotaxis (Figure 6G-H), while AMD3100 did not prevent CD8+ migration towards CXCL12 (Figure 6I). These data support the view that differential expression of CXCR4 may selectively affect the intratumoral trafficking of regulatory versus effector cells towards intratumoral CXCL12 gradients.

CXCL12/CXCR4 antagonism using AMD3100 selectively impacts T-regs infiltration in a second murine tumor model

To test the impact of CXCL12/CXCR4 axis blockade on T-regs infiltration in a second solid tumor, we employed the B16F10 murine melanoma model. Previous reports reveal that B16 melanoma cells express both CXCR4 and CXCL12 (41) and have assessed the effect of CXCR4 antagonists on tumor spread (10). To test the effect of CXCL12/CXCR4 manipulation on T-cell infiltration into melanomas, osmotic pumps delivering AMD3100 were implanted as described in the Methods section. We observed a significant decrease of CD4+CD25+ and CD4+CD25+FoxP3+ T-cells in the AMD3100 treated tumors compared to controls (1277.28 ± 36.73 T-cells/g and 202.56 ± 29.14 T-cells/g vs. 3494.27 ± 831.46 T-cells/g and 573.55 ± 111.40 T-cells/g $P < 0.05$, Figure 7A), while the CD8+ TIL count was not significantly different between the experimental group and controls (1569.28 ± 599.99 T-cells/g vs. 3337.51 ± 687.12 T-cells/g, $P = 0.89$, Figure 7A). Intratumoral T-regs were shown to express higher levels of CXCR4 compared to CD8+ cells (Figure 7B). These data are consistent with those generated in the ovarian cancer model and supports the view that the antagonism of the CXCR4/CXCL12 axis results in selective T-reg depletion compared to CD8+ T-cells potentially as a result of higher levels of CXCR4 expression on the

regulatory T-cell subpopulation. Tumor growth delay at the levels of 4 and 8 times the initial volume was 2.9 ± 0.6 days and 4.7 ± 1.5 days in control tumors (n=11), and 2.7 ± 0.7 days and 4.3 ± 1.5 days in AMD treated tumors (n=12), respectively. There was no significant difference in the rate of tumor growth or in overall survival between the groups, which is consistent with reports that the CXCL12/CXCR4 axis does not impact B16F10 melanoma cell proliferation(42) and that depletion of T-regs alone is not sufficient to promote tumor eradication in the B16 melanoma model.

Discussion

This first-of-its-kind study confirms that blockade of the CXCR4/CXCL12 axis alone can reduce ovarian tumor growth and peritoneal dissemination, resulting in a significant survival advantage in immunocompetent mice. The murine model that was used reproduces a clinical sequence of events from the detection of ascites to the appearance of disseminated intraperitoneal disease that resembles the progression of the most common form of papillary epithelial ovarian cancer in humans 28). In this context, we investigated the ability of the CXCL12/CXCR4 axis blockade to target multiple aspects of tumor progression, including cancer growth, angiogenesis, and tumor-specific immune-dysregulation.

This study confirmed that CXCL12 directly impacts cancer cell proliferation in this model(13, 14, 16, 43). When CXCL12 was knocked-down in BR5-1 cells, which natively express both CXCL12 and CXCR4, we observed a deceleration of tumor growth in vivo and a significant reduction in tumor cell proliferation in vitro that was reversed by adding exogenous CXCL12 (21). Furthermore, AMD3100-treated tumors had increased tumor cell apoptosis and tumor necrosis compared to controls, which is consistent with published data demonstrating that AMD3100-treatment can abrogate CXCL12-mediated protection by apoptosis in cancer 44,45) and reduce the number of intraperitoneal masses in nude mice(21).

Tumor-derived CXCL12 plays a part in the trafficking of pro-angiogenic cells (i.e., plasmacytoid dendritic cell) and the induction of pro-angiogenic factors (i.e. CCL8) in the tumor microenvironment(46). VEGF and CXCL12 have been shown to act synergistically to induce CXCR4 expression and migration of vascular endothelial cells(19). In this study, impaired vascularization in the RNAi and AMD3100 treatment groups was observed. Tumor angiogenesis is also known to contribute to tumor immune escape through multiple mechanisms, including suppression of adhesion molecule expression, reduction of tumor-specific CTL function and APC activation, and induction of intratumoral T-reg localization(47,48). Therefore the anti-angiogenic effect that AMD3100 elicited in this study may be associated with a reduction of both tumor growth and dissemination as well as a partial correction of tumor immunity.

This model of ovarian cancer in an immunocompetent mouse, allowed us to demonstrate for the first time that AMD3100 results in a significant and selective 4- to 5-fold reduction of FoxP3+ cells in ovarian tumors that was not associated with either a change in the distribution of T-regs in other organs (i.e., spleen and thymus) or a diminution of intratumoral CD8+ T-cells. CXCL12-mediated mechanisms hypothesized to be involved in immune suppression are either the repulsion of anti-tumor effector T-cells or the active recruitment of immunosuppressive cells (25,39). The preferential accumulation of tumor-specific, T-cell suppressive T-regs in ovarian cancer tissue and ascites was previously correlated with poor survival(49). Our results show that AMD3100 differentially blocks intratumoral T-reg infiltration and migration in comparison to CD8+ T-cells in vivo and in vitro, respectively. We also found that this was associated with the finding that intratumoral T-regs express significantly higher levels of CXCR4 than CD8+ T-cells. These findings

were recapitulated in a second tumor model(49). Furthermore, we demonstrated that depletion of T-regs from TILs reversed an apparent immunosuppressive effect on tumor antigen specific Granzyme B production in vitro, supporting the concept that exclusion of T-regs from the intratumoral milieu may augment local anti-tumor immunity(50).

These findings reveal a new mechanism for modulating intra-tumoral T-cell subsets that compares favorably with other therapeutic strategies. In this study, AMD3100 treatment resulted in a 6-fold increase in the intratumoral Teff/Treg ratio. This highly significant change was associated with significantly improved cytotoxic T-cell function in tumor tissue, prolonged survival in this model and is consistent with recent approaches to depleting intratumoral T-regs (51,52). Tube, S. et al. reported that the CD8/Treg ratio in TC-1/anti-CTLA-4-gamma1 expressing tumors was increased by 6.5-fold compared to control TC-1 tumors(52). Yoshimura K. et al. reported that administration of an engineered hepatic-targeting Listeria monocytogenes (LM) with cyclophosphamide lead to a 5-fold increase in the Teff/Treg ratio in a murine model of colorectal cancer metastasis to the liver(51). Importantly, we clearly demonstrated that the CXCR4 antagonism induced selective reduction of intratumoral T-regs without affecting systemic T-regs and intratumoral CD8+ T effector cells. Conventional strategies to reduce the number of intratumoral T-regs including the systemic application of anti-CD25 antibody and cyclophosphamide do not specifically target T-regs, and therefore also deplete T effector cells. Furthermore, such strategies have significant drawbacks, including toxicity and induction of autoimmunity due to the systemic elimination of T-regs(53). In our study we have successfully identified an effective strategy to selectively deplete intratumoral T-regs, resulting in prolonged survival in a murine model of ovarian cancer.

In summary, these data generated in an immunocompetent syngeneic and orthotopic murine model, lend important support to the view that the CXCL12/CXCR4 axis plays multiple roles in the pathogenesis of ovarian cancer. This study, demonstrates a new role for this axis in the selective trafficking of T-regs into the tumor in addition to reaffirming its established roles in tumor apoptosis, growth and angiogenesis. We also show that these multimodal effects of specific single agent CXCR4/CXCL12 axis blockade in this model of ovarian cancer are associated with a signficantly prolonged survival and reductions in indices of tumor progression. The availability of a safe, effective and clinically applicable CXCR4 antagonist in AMD3100 adds both to the direct clinical translatability of this study and to the enthusiasm amongst clinicians to explore the use of this agent as an adjunct to conventional chemotherapy, including taxol in platinum resistant disease, or in combination with other immunotherapies aimed at enhancing CD8+ T-cell responses in human ovarian cancer.

Supplementary Material

Refer to Web version on PubMed Central for supplementary material.

Acknowledgments

We thank Dr. Gebremichael at the Harvard School of Public Health for help with the independent statistical analysis of datasets. We thank Christine Linton, Brett Kodish, Haaris Beg, and Federico Ivaldi for technical support.

MCP and ER were supported by Public Health Service Grants RO1 AI49757, the Marsha Rivkin Center for Ovarian Cancer Research, and philanthropic funds. SO was supported by the Marsha Rivkin Center for Ovarian Cancer Research and the Garber Award.

References

1. Kulbe H, Thompson R, Wilson JL, Robinson S, Hagemann T, Fatah R, et al. The inflammatory cytokine tumor necrosis factor-alpha generates an autocrine tumor-promoting network in epithelial ovarian cancer cells. Cancer Res. 2007; 67:585–92. [PubMed: 17234767]
2. Milliken D, Scotton C, Raju S, Balkwill F, Wilson J. Analysis of chemokines and chemokine receptor expression in ovarian cancer ascites. Clin Cancer Res. 2002; 8:1108–14. [PubMed: 11948121]
3. Negus RP, Stamp GW, Hadley J, Balkwill FR. Quantitative assessment of the leukocyte infiltrate in ovarian cancer and its relationship to the expression of C-C chemokines. Am J Pathol. 1997; 150:1723–34. [PubMed: 9137096]
4. Ochsenbein AF. Principles of tumor immunosurveillance and implications for immunotherapy. Cancer Gene Ther. 2002; 9:1043–55. [PubMed: 12522443]
5. Schimanski CC, Galle PR, Moehler M. Chemokine receptor CXCR4-prognostic factor for gastrointestinal tumors. World J Gastroenterol. 2008; 14:4721–4. [PubMed: 18720530]
6. Webb TJ, Giuntoli RL 2nd, Rogers O, Schneck J, Oelke M. Ascites specific inhibition of CD1d-mediated activation of natural killer T-cells. Clin Cancer Res. 2008; 14:7652–8. [PubMed: 19047090]
7. Balkwill F. The significance of cancer cell expression of the chemokine receptor CXCR4. Semin Cancer Biol. 2004; 14:171–9. [PubMed: 15246052]
8. Muller A, Homey B, Soto H, Ge N, Catron D, Buchanan ME, et al. Involvement of chemokine receptors in breast cancer metastasis. Nature. 2001; 410:50–6. [PubMed: 11242036]
9. Jaafar F, Righi E, Lindstrom V, Linton C, Nohadani M, Van Noorden S, et al. Correlation of CXCL12 expression and FoxP3+ cell infiltration with human papillomavirus infection and clinicopathological progression of cervical cancer. Am J Pathol. 2009; 175:1525–35. [PubMed: 19808652]
10. Lee CH, Kakinuma T, Wang J, Zhang H, Palmer DC, Restifo NP, et al. Sensitization of B16 tumor cells with a CXCR4 antagonist increases the efficacy of immunotherapy for established lung metastases. Mol Cancer Ther. 2006; 5:2592–9. [PubMed: 17041104]
11. Marchesi F, Monti P, Leone BE, Zerbi A, Vecchi A, Piemonti L, et al. Increased survival, proliferation, and migration in metastatic human pancreatic tumor cells expressing functional CXCR4. Cancer Res. 2004; 64:8420–7. [PubMed: 15548713]
12. Smith MC, Luker KE, Garbow JR, Prior JL, Jackson E, Piwnica-Worms D, et al. CXCR4 regulates growth of both primary and metastatic breast cancer. Cancer Res. 2004; 64:8604–12. [PubMed: 15574767]
13. Zhou Y, Larsen PH, Hao C, Yong VW. CXCR4 is a major chemokine receptor on glioma cells and mediates their survival. J Biol Chem. 2002; 277:49481–7. [PubMed: 12388552]
14. Scotton C, Milliken D, Wilson J, Raju S, Balkwill F. Analysis of CC chemokine and chemokine receptor expression in solid ovarian tumours. Br J Cancer. 2001; 85:891–7. [PubMed: 11556842]
15. Scotton CJ, Wilson JL, Milliken D, Stamp G, Balkwill FR. Epithelial cancer cell migration: a role for chemokine receptors? Cancer Res. 2001; 61:4961–5. [PubMed: 11431324]
16. Scotton CJ, Wilson JL, Scott K, Stamp G, Wilbanks GD, Fricker S, et al. Multiple actions of the chemokine CXCL12 on epithelial tumor cells in human ovarian cancer. Cancer Res. 2002; 62:5930–8. [PubMed: 12384559]
17. Helbig G, Christopherson KW 2nd, Bhat-Nakshatri P, Kumar S, Kishimoto H, Miller KD, et al. NF-kappaB promotes breast cancer cell migration and metastasis by inducing the expression of the chemokine receptor CXCR4. J Biol Chem. 2003; 278:21631–8. [PubMed: 12690099]
18. Kukreja P, Abdel-Mageed AB, Mondal D, Liu K, Agrawal KC. Up-regulation of CXCR4 expression in PC-3 cells by stromal-derived factor-1alpha (CXCL12) increases endothelial adhesion and transendothelial migration: role of MEK/ERK signaling pathway-dependent NF-kappaB activation. Cancer Res. 2005; 65:9891–8. [PubMed: 16267013]
19. Kryczek I, Lange A, Mottram P, Alvarez X, Cheng P, Hogan M, et al. CXCL12 and vascular endothelial growth factor synergistically induce neoangiogenesis in human ovarian cancers. Cancer Res. 2005; 65:465–72. [PubMed: 15695388]

20. Kryczek I, Wei S, Keller E, Liu R, Zou W. Stroma-derived factor (SDF-1/CXCL12) and human tumor pathogenesis. Am J Physiol Cell Physiol. 2007; 292:C987–95. [PubMed: 16943240]
21. Kajiyama H, Shibata K, Terauchi M, Ino K, Nawa A, Kikkawa F. Involvement of SDF-1alpha/CXCR4 axis in the enhanced peritoneal metastasis of epithelial ovarian carcinoma. Int J Cancer. 2008; 122:91–9. [PubMed: 17893878]
22. Dunussi-Joannopoulos K, Zuberek K, Runyon K, Hawley RG, Wong A, Erickson J, et al. Efficacious immunomodulatory activity of the chemokine stromal cell-derived factor 1 (SDF-1): local secretion of SDF-1 at the tumor site serves as T-cell chemoattractant and mediates T-cell-dependent antitumor responses. Blood. 2002; 100:1551–8. [PubMed: 12176869]
23. Youn JI, Nagaraj S, Collazo M, Gabrilovich DI. Subsets of myeloid-derived suppressor cells in tumor-bearing mice. J Immunol. 2008; 181:5791–802. [PubMed: 18832739]
24. Zou W, Machelon V, Coulomb-L'Hermin A, Borvak J, Nome F, Isaeva T, et al. Stromal-derived factor-1 in human tumors recruits and alters the function of plasmacytoid precursor dendritic cells. Nat Med. 2001; 7:1339–46. [PubMed: 11726975]
25. Vianello F, Papeta N, Chen T, Kraft P, White N, Hart WK, et al. Murine B16 melanomas expressing high levels of the chemokine stromal-derived factor-1/CXCL12 induce tumor-specific T-cell chemorepulsion and escape from immune control. J Immunol. 2006; 176:2902–14. [PubMed: 16493048]
26. Devine SM, Flomenberg N, Vesole DH, Liesveld J, Weisdorf D, Badel K, et al. Rapid mobilization of CD34+ cells following administration of the CXCR4 antagonist AMD3100 to patients with multiple myeloma and non-Hodgkin's lymphoma. J Clin Oncol. 2004; 22:1095–102. [PubMed: 15020611]
27. Liles WC, Broxmeyer HE, Rodger E, Wood B, Hubel K, Cooper S, et al. Mobilization of hematopoietic progenitor cells in healthy volunteers by AMD3100, a CXCR4 antagonist. Blood. 2003; 102:2728–30. [PubMed: 12855591]
28. Xing D, Orsulic S. A mouse model for the molecular characterization of brca1-associated ovarian carcinoma. Cancer Res. 2006; 66:8949–53. [PubMed: 16982732]
29. Fidler IJ. Selection of successive tumour lines for metastasis. Nat New Biol. 1973; 242:148–9. [PubMed: 4512654]
30. Kashiwagi S, Izumi Y, Gohongi T, Demou ZN, Xu L, Huang PL, et al. NO mediates mural cell recruitment and vessel morphogenesis in murine melanomas and tissue-engineered blood vessels. J Clin Invest. 2005; 115:1816–27. [PubMed: 15951843]
31. Santosuosso M, McCormick S, Roediger E, Zhang X, Zganiacz A, Lichty BD, et al. Mucosal luminal manipulation of T-cell geography switches on protective efficacy by otherwise ineffective parenteral genetic immunization. J Immunol. 2007; 178:2387–95. [PubMed: 17277145]
32. Singh R, Paterson Y. Vaccination strategy determines the emergence and dominance of CD8+ T-cell epitopes in a FVB/N rat HER-2/neu mouse model of breast cancer. Cancer Res. 2006; 66:7748–57. [PubMed: 16885378]
33. Poznansky MC, Olszak IT, Foxall R, Evans RH, Luster AD, Scadden DT. Active movement of T-cells away from a chemokine. Nat Med. 2000; 6:543–8. [PubMed: 10802710]
34. Bast RC Jr. Hennessy B, Mills GB. The biology of ovarian cancer: new opportunities for translation. Nat Rev Cancer. 2009; 9:415–28. [PubMed: 19461667]
35. Datema R, Rabin L, Hincenbergs M, Moreno MB, Warren S, Linquist V, et al. Antiviral efficacy in vivo of the anti-human immunodeficiency virus bicyclam SDZ SID 791 (JM 3100), an inhibitor of infectious cell entry. Antimicrob Agents Chemother. 1996; 40:750–4. [PubMed: 8851605]
36. Mirshahi F, Pourtau J, Li H, Muraine M, Trochon V, Legrand E, et al. SDF-1 activity on microvascular endothelial cells: consequences on angiogenesis in in vitro and in vivo models. Thromb Res. 2000; 99:587–94. [PubMed: 10974345]
37. Hartmann TN, Burger JA, Glodek A, Fujii N, Burger M. CXCR4 chemokine receptor and integrin signaling co-operate in mediating adhesion and chemoresistance in small cell lung cancer (SCLC) cells. Oncogene. 2005; 24:4462–71. [PubMed: 15806155]
38. Muller A, Sonkoly E, Eulert C, Gerber PA, Kubitza R, Schirlau K, et al. Chemokine receptors in head and neck cancer: association with metastatic spread and regulation during chemotherapy. Int J Cancer. 2006; 118:2147–57. [PubMed: 16331601]

39. Zou L, Barnett B, Safah H, Larussa VF, Evdemon-Hogan M, Mottram P, et al. Bone marrow is a reservoir for CD4+CD25+ regulatory T-cells that traffic through CXCL12/CXCR4 signals. Cancer Res. 2004; 64:8451–5. [PubMed: 15548717]
40. Sato E, Olson SH, Ahn J, Bundy B, Nishikawa H, Qian F, et al. Intraepithelial CD8+ tumor-infiltrating lymphocytes and a high CD8+/regulatory T-cell ratio are associated with favorable prognosis in ovarian cancer. Proc Natl Acad Sci U S A. 2005; 102:18538–43. [PubMed: 16344461]
41. van der Meulen AA, Biber K, Lukovac S, Balasubramaniyan V, den Dunnen WF, Boddeke HW, et al. The role of CXC chemokine ligand (CXCL)12-CXC chemokine receptor (CXCR)4 signalling in the migration of neural stem cells towards a brain tumour. Neuropathol Appl Neurobiol. 2009; 35:579–91. [PubMed: 19627512]
42. Sun X, Cheng G, Hao M, Zheng J, Zhou X, Zhang J, et al. CXCL12 / CXCR4 / CXCR7 chemokine axis and cancer progression. Cancer Metastasis Rev. 2010; 29:709–22. [PubMed: 20839032]
43. Sehgal A, Keener C, Boynton AL, Warrick J, Murphy GP. CXCR-4, a chemokine receptor, is overexpressed in and required for proliferation of glioblastoma tumor cells. J Surg Oncol. 1998; 69:99–104. [PubMed: 9808513]
44. Barbero S, Bonavia R, Bajetto A, Porcile C, Pirani P, Ravetti JL, et al. Stromal cell-derived factor 1alpha stimulates human glioblastoma cell growth through the activation of both extracellular signal-regulated kinases 1/2 and Akt. Cancer Res. 2003; 63:1969–74. [PubMed: 12702590]
45. Redjal N, Chan JA, Segal RA, Kung AL. CXCR4 inhibition synergizes with cytotoxic chemotherapy in gliomas. Clin Cancer Res. 2006; 12:6765–71. [PubMed: 17121897]
46. Curiel TJ, Cheng P, Mottram P, Alvarez X, Moons L, Evdemon-Hogan M, et al. Dendritic cell subsets differentially regulate angiogenesis in human ovarian cancer. Cancer Res. 2004; 64:5535–8. [PubMed: 15313886]
47. Li B, Lalani AS, Harding TC, Luan B, Koprivnikar K, Huan Tu G, et al. Vascular endothelial growth factor blockade reduces intratumoral regulatory T-cells and enhances the efficacy of a GM-CSF-secreting cancer immunotherapy. Clin Cancer Res. 2006; 12:6808–16. [PubMed: 17121902]
48. Manning EA, Ullman JG, Leatherman JM, Asquith JM, Hansen TR, Armstrong TD, et al. A vascular endothelial growth factor receptor-2 inhibitor enhances antitumor immunity through an immune-based mechanism. Clin Cancer Res. 2007; 13:3951–9. [PubMed: 17606729]
49. Curiel TJ, Coukos G, Zou L, Alvarez X, Cheng P, Mottram P, et al. Specific recruitment of regulatory T-cells in ovarian carcinoma fosters immune privilege and predicts reduced survival. Nat Med. 2004; 10:942–9. [PubMed: 15322536]
50. Chen YL, Fang JH, Lai MD, Shan YS. Depletion of CD4(+)CD25(+) regulatory T-cells can promote local immunity to suppress tumor growth in benzo[a]pyrene-induced forestomach carcinoma. World J Gastroenterol. 2008; 14:5797–809. [PubMed: 18855977]
51. Yoshimura K, Laird LS, Chia CY, Meckel KF, Slansky JE, Thompson JM, et al. Live attenuated Listeria monocytogenes effectively treats hepatic colorectal cancer metastases and is strongly enhanced by depletion of regulatory T-cells. Cancer Res. 2007; 67:10058–66. [PubMed: 17942940]
52. Tuve S, Chen BM, Liu Y, Cheng TL, Toure P, Sow PS, et al. Combination of tumor site-located CTL-associated antigen-4 blockade and systemic regulatory T-cell depletion induces tumor-destructive immune responses. Cancer Res. 2007; 67:5929–39. [PubMed: 17575163]
53. Colombo MP, Piconese S. Regulatory-T-cell inhibition versus depletion: the right choice in cancer immunotherapy. Nat Rev Cancer. 2007; 7:880–7. [PubMed: 17957190]

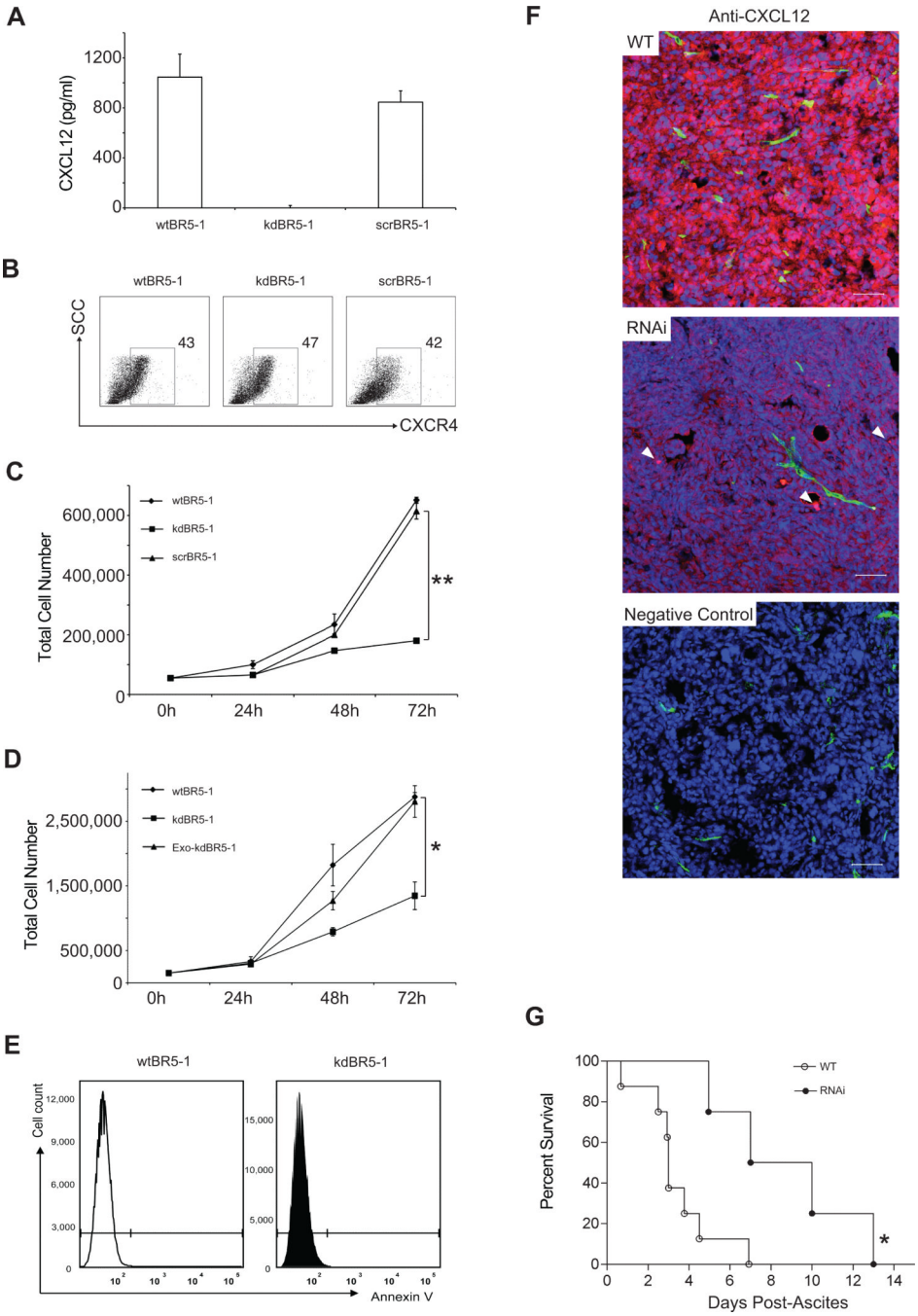

Figure 1.

Effect of CXCL12 knockdown on cell proliferation in vitro and in vivo (A) CXCL12 ELISA results from cell supernatants of wtBR5-1, kdBR5-1, and scrBR5-1(mean ± SEM, n = 3). (B) Cell surface expression of CXCR4 on wtBR5-1, kdBR5-1, and scrBR5-1 cells (n=3). (C) Proliferation curves comparing CXCL12-producing cells, wtBR5-1 and scrBR5-1, kdBR5-1, ***P*<0.001(mean ± SEM, n=3). (D)Proliferation curves of wtBR5-1 and kdBR5-1 cells in standard media(DMEM with 10% FBS) and RNAi cells in media containing 100ng/ml of exogenous recombinant CXCL12(Exo CXCL12) **P* < 0.005. (E)Annexin V staining of wtBR5-1 and kdBR5-1 cells(n=3). (F)Confocal imaging of CXCL12 expression(red) in WT vs. RNAi tumors in vivo. Perfused vessels(green)(fluorescein-labeled lectin) and

nuclear counterstaining(blue)(To-Pro-3). In the RNAi image CXCL12 stromal expression indicated by arrows. Scale bar:50 μm. (G)Kaplan-Meier survival analysis. FBV/NJ mice were followed up for appearance of ascites and tumor progression to endpoint described in Methods section for wtBR5-1(WT) vs. kdBR5-1(RNAi) tumor(four to six mice, two independent experiments, *$P < 0.05$).

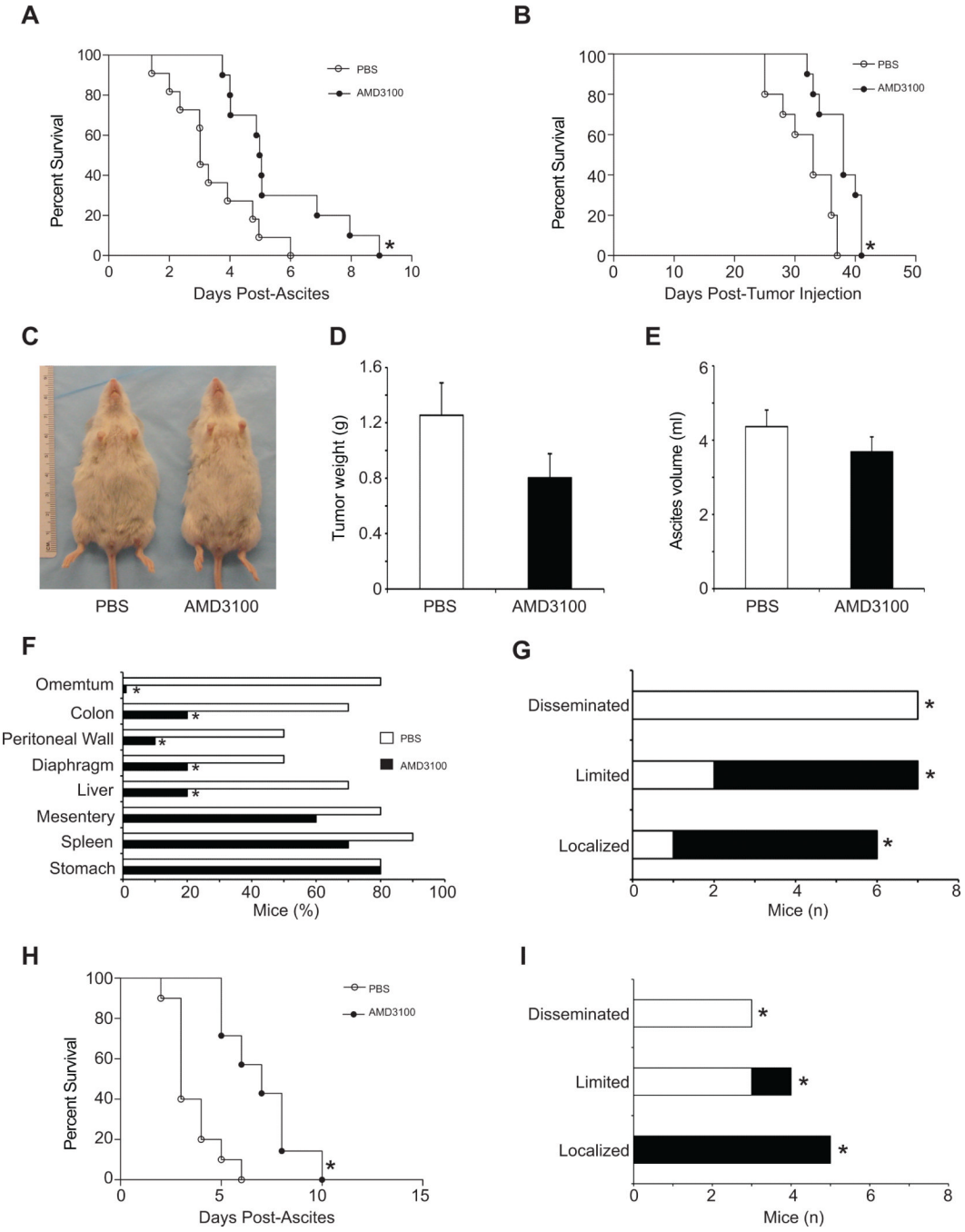

Figure 2.

Effect of AMD3100 treatment on tumor progression and mice survival. (A-G)AMD3100 or PBS was delivered into FVB/NJ mice with wtBR5-1 tumors at onset of ascites(schedule A). (A-B) Survival curves (A) from the onset of ascites and (B) from the time of tumor cell injection. (n = 10 per group,*P<0.05). (C-E)Effect of AMD3100 treatment on tumor weight and ascites formation. Tumor bearing mice were treated with AMD3100 or PBS under schedule A (n = 8 from three experiments) and euthanized at day 3 post ascites. (C)Representative mice from AMD3100 and PBS groups are shown. (D)Total tumor weight and (E)ascites volumes were measured. (F)Bar graph representing the percentage of mice with visible tumor deposits on organs at necropsy (n=10 per group;*P<0.01). (G) Tumor

dissemination. Classification: localized (localizations≤3), limited (6<localizations>3, with no visible masses on mesentery and diaphragm), and disseminated (localizations≥6 including mesentery and diaphragm localization), *P<0.01. (H-I)AMD3100 or control PBS delivered for 15 days after tumor cell injection (schedule B). (H)Survival curves of the mice treated under schedule B from the onset of ascites showing that AMD3100 treated mice increased survival window(n=6, *P<0.01) and (I)reduced tumor dissemination (n=6, P<0.05).

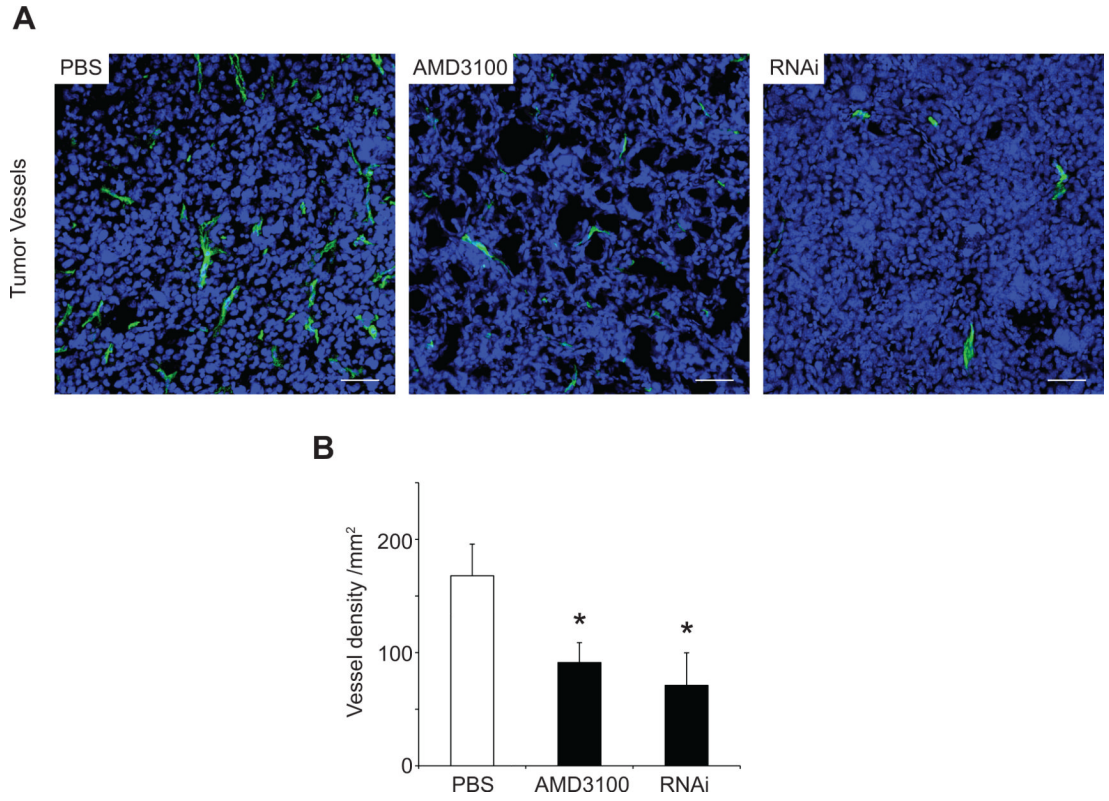

Figure 3.

Effect of CXCL12/CXCR4 manipulation on tumor angiogenesis. (A)Confocal imaging of tumor angiogenesis from PBS(n = 8), AMD3100(n = 8), and RNAi(n = 6) tumors. Functional vessels are visible in green, and blue represents nuclear counterstaining (To-Pro-3). Scale bars: 50μm. (B)Vessel quantitation expressed as density per mm^2. Microvascular density was quantified from five randomized fields using Image J, and expressed as average±SEM, *P<0.05.

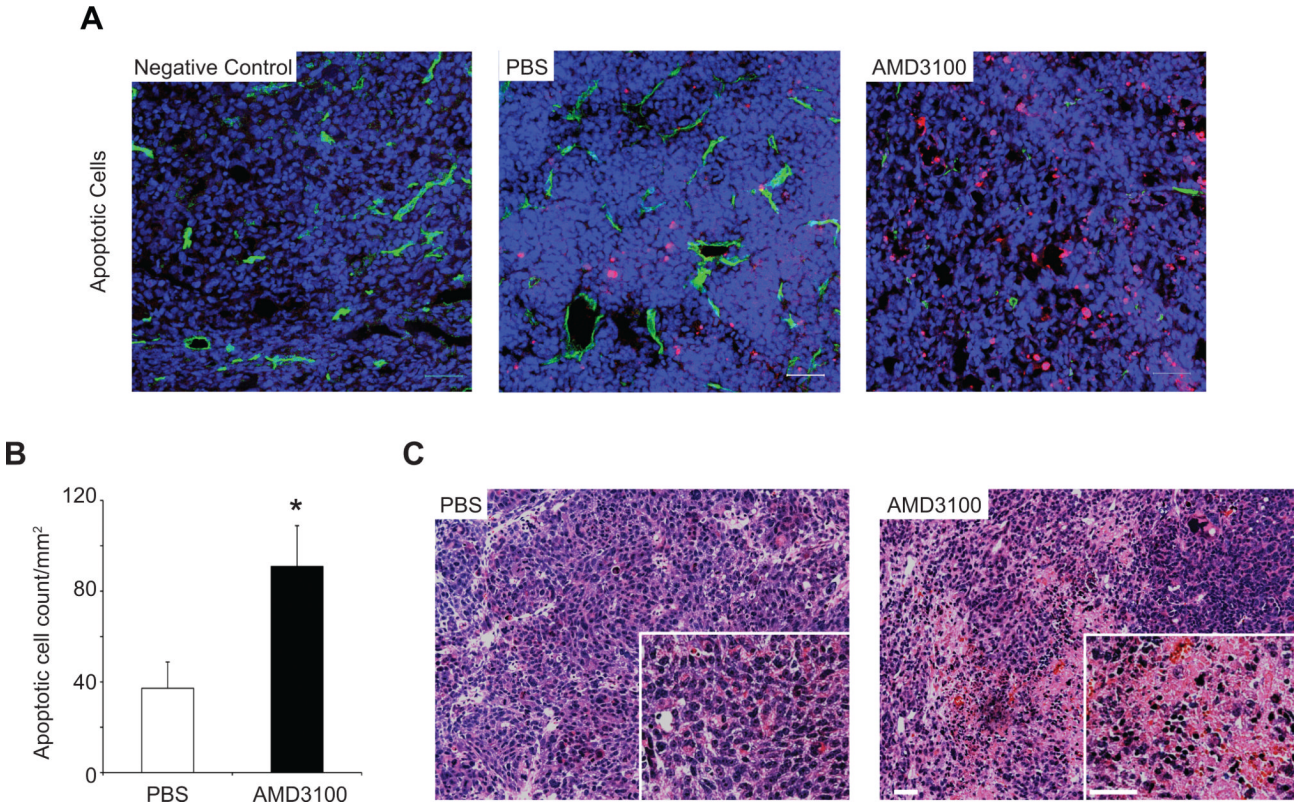

Figure 4.

(A)Confocal imaging of tumor apoptosis in tumor bearing mice treated with AMD3100(n = 8) or PBS(n = 7)(schedule A). Vessels(green) and nuclei(blue) were visualized(To-Pro-3). Apoptotic cells(red) were identified using TUNEL staining. (B)quantified from five randomized fields using Image J, **P*<0.05. (C)H&E staining of PBS and AMD3100 tumor sections demonstrating necrosis in AMD3100 tumors. Scale bar:50μm.

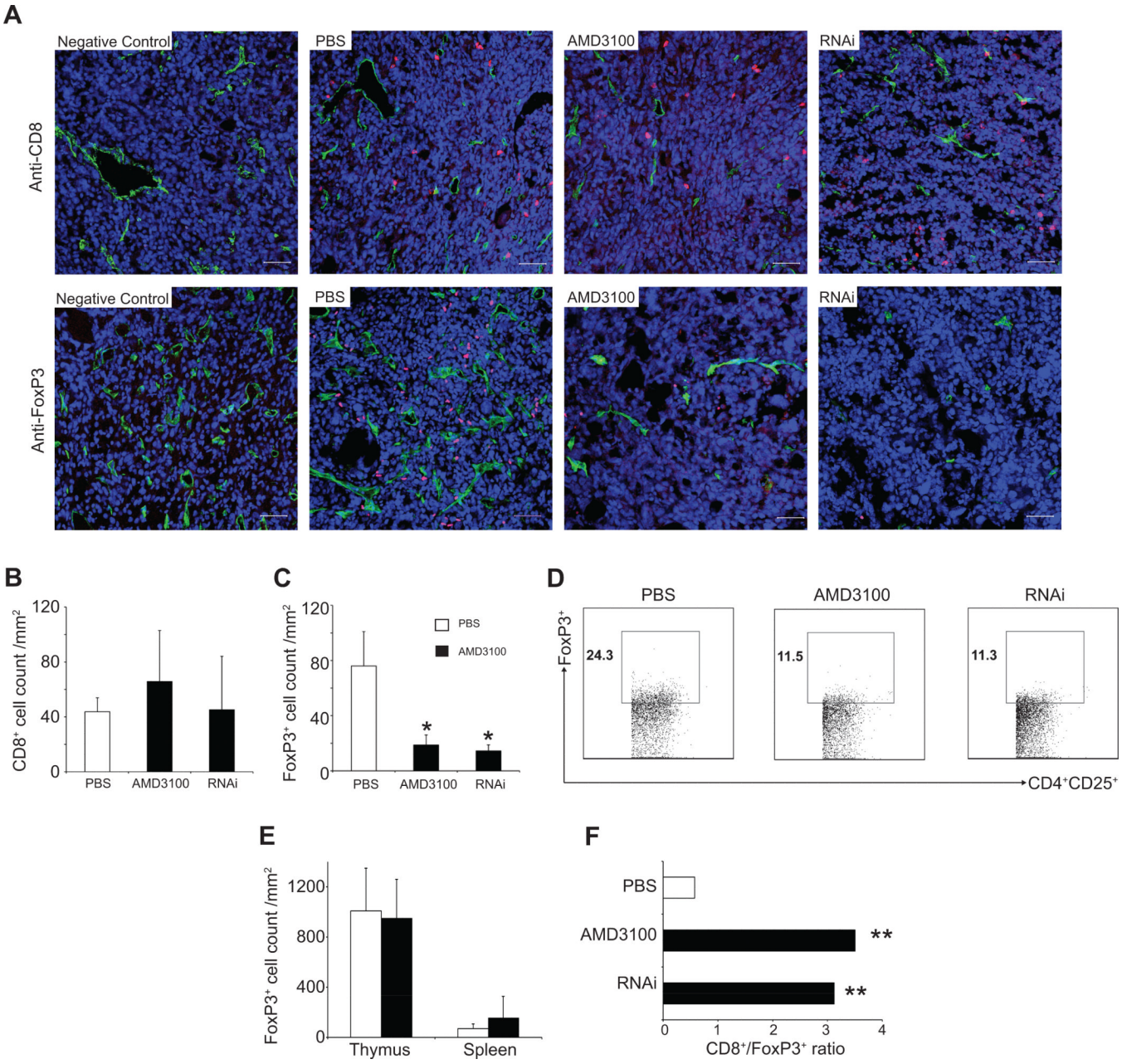

Figure 5.

(A-C)Effect of CXCL12/CXCR4 manipulation on intratumoral FoxP3+ and CD8+ lymphocyte infiltration.(A), upper panels; confocal imaging of intratumoral CD8+ cells(red) from PBS(n=7), AMD3100(n=7), and RNAi(n=5) tumors. (A), lower panels; confocal imaging of intratumoral FoxP3+ cells(red) from PBS(n= 3), AMD3100(n = 11), and RNAi(n=7) tumors vessels(green) and nuclei(blue). Scale bars: 50μm. The number of CD8+ and FoxP3+ cells was quantified from five randomized fields, **P*<0.05. (B)CD8+ cell, (C)FoxP3+ count. (D) Representative results of three independent flow analyses on four to six mice per group and reported as percentage of CD4+CD25+FoxP3+ TILs(450,000 events collected). TILs were stained with anti-CD4, anti-CD25, and anti-FoxP3. (E) FoxP3+ cell count per mm^2 from thymus and spleen(n = 3). (F)CD8+/FoxP3+ ratios, ***P*<0.01.

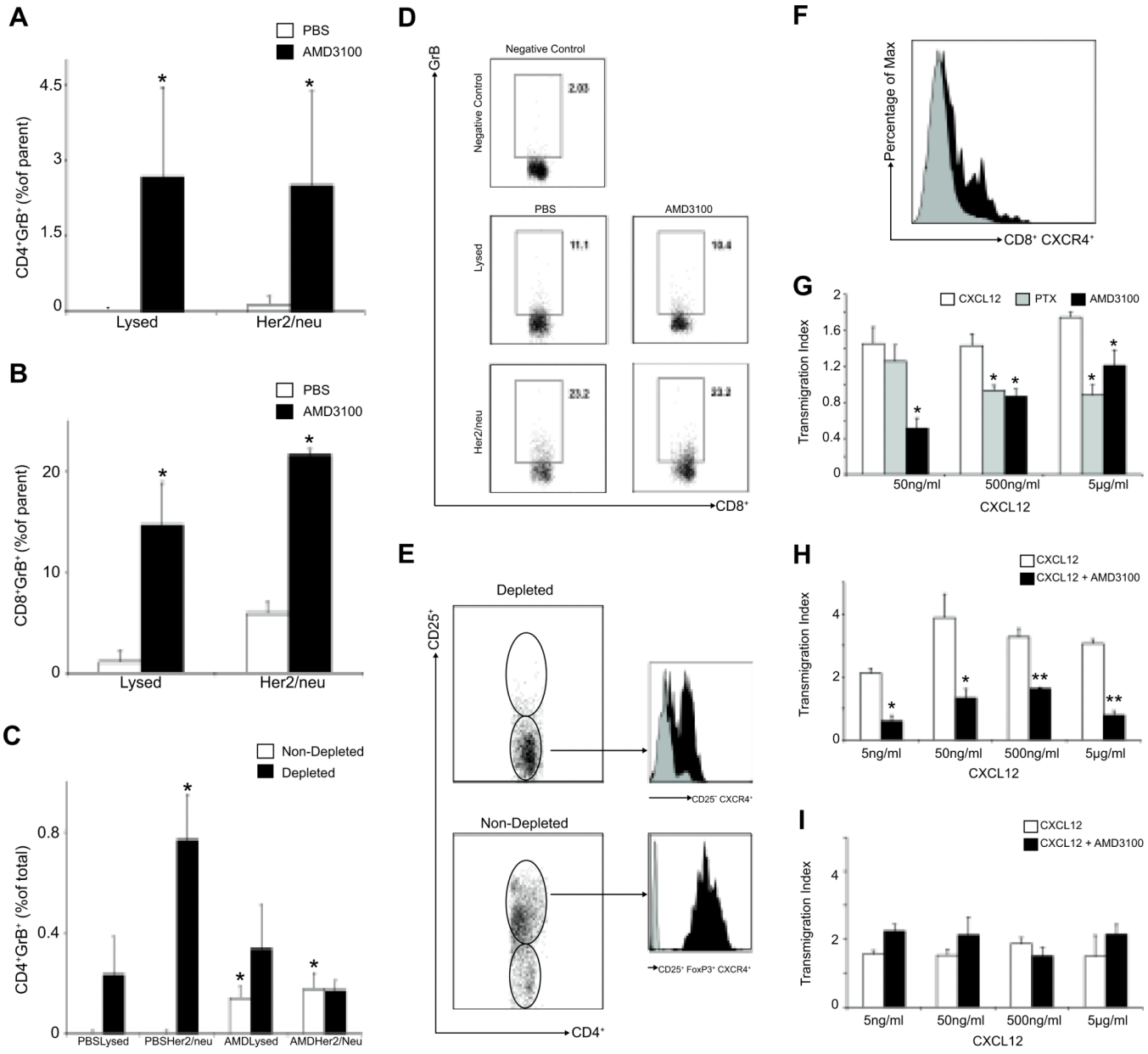

Figure 6.

Effect of tumor-specific T-cell function and migration after AMD3100 treatment. (A-B) TILs from AMD3100 and PBS groups were stimulated with tumor lysates(Lysed) or Her2/neu peptide(Her2/neu)(n=3 per group, 450,000 flow events collected). Results are reported as difference between non-stimulated(media alone) and stimulated cells and expressed as frequency of parent CD4+(A) or CD8+ cells(B), **P*<0.05. (C)TILs were depleted of T-regs and stimulated for 24hr. Granzyme B production was measured(n = 6 per group, 450,000 flow events collected). Results are reported as difference between non-stimulated(media) and stimulated, adjusted for the number of CD4+ cells in depleted and non-depleted groups, and reported as percentage of total CD4+ cells, **P*<0.05. (D)Representative flow data relating to T-cell function in splenocytes from PBS and AMD3100 groups showing no difference in Granzyme B production in CD8+ cells per each stimulation condition(350,000 events per condition). (E) Expression of CXCR4 on intratumoral non-

depleted(CD4+CD25+FoxP3+), depleted cells (CD4+CD25−) or (F) on CD8+ cells. CXCL12 induced transmigration of tumor derived T-regs(G and H) and intratumoral CD8+ cells(I). T-regs migration to CXCL12 was tested in a transwell assay. Mean ± SEM of three wells from five experiments are shown. Transmigration index was calculated as the ratio between migrated cells in the lower chambers and the average of the random migrated cells (media alone in the upper and lower chambers) ± SEM. **P*<0.05, ***P*<0.005.

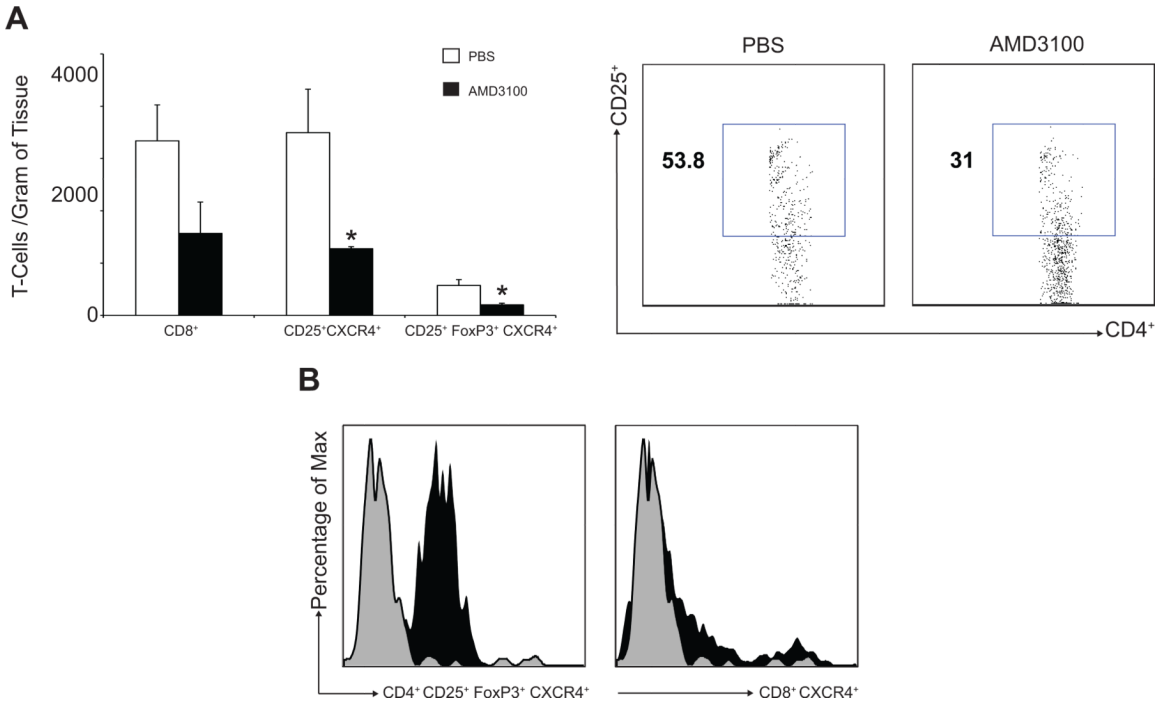

Figure 7.

Effect of AMD3100 on B16F10 subcutaneous tumors in C57/BL6 mice. (A)Intratumoral CD8+ cells(n=6) and T-regs infiltration(n=6) was assessed by flow cytometry(750,000 events) and expressed as number of cells/gram of tumor. (B)Lower CXCR4 expression was shown on intratumoral T-regs cells (left panel) compared to T-effector cells (right panel) (1×10^6 events recorded)(representative histograms shown).